Rotation-translation coupling of soft objects in lubricated contact

Soft Matter

Rotation-translation coupling of soft objects in lubricated contact

Arash Kargar-Estahbanati,[a] and Bhargav Rallabandi,[*a]

We study the coupling between rotation and translation of a submerged cylinder in lubricated contact with a soft elastic substrate. Using numerical solutions and asymptotic theory, we analyze the elasto-hydrodynamic problem over the entire range of substrate deformations relative to the thickness of the intervening fluid film. We find a strong coupling between the rotation and translation of the cylinder when the surface deformation of the substrate is comparable to the thickness of the lubricating fluid layer. In the limit of large deformations, we show that the bodies are in near-Hertzian contact and cylinder rolls without slip, reminiscent of dry frictional contact. When the surface deformation is small relative to the separation between the surfaces, the coupling persists but is weaker, and the rotation rate scales with the translation speed to the one-third power. We then show how the external application of a torque modifies these behaviors by generating different combinations of rotational and translational motions, including back-spinning and top-spinning states. We demonstrate that these behaviors are robust regardless of whether the elastic substrate is thick or thin relative to the length scales of the flow.

1 Introduction

Lubricating two contacting surfaces in relative motion with an intervening viscous fluid can reduce wear by lowering friction[1]. Classical studies of lubricated contacts focused on metal surfaces, due to their application in bearings[2,3] and pistons[4,5]. In recent years, however, the popularity of soft materials has drawn attention to soft lubricated contacts where at least one of the contacting surfaces is deformed significantly by the contact pressure. The basic principles of soft lubrication are also relevant in applications such as biomechanics of synovial joints[6], the motion of blood cells in capillaries[7], eggs through the oviduct[8], and particles moving in soft channels[9] or near elastic membranes[10], to name a few.

The tight coupling between elasticity of the contacting solids and the intervening fluid flow allows soft lubricated systems to support both normal and tangential applied forces. Experimental studies of soft lubricated flows have used both interferometry[11–13] and contactless mechanical probes[14,15]. Theoretical treatments typically require numerical analysis[16,17], although analytical solutions are available in asymptotic limits. In the limit of large normal loads, the geometry approaches that of classical Hertzian contact[18,19], separated only by an extremely thin film of fluid supported by the relative motion of the surfaces[20,21]. In the opposite limit of small normal loads, the surfaces slide with

a relatively thick fluid film and the surfaces are only slightly deformed[22–24]. These ideas have been quantified experimentally and theoretically both for soft objects and for rigid objects with soft coatings. Previous work has studied soft substrates much thicker than typical length scales of the flow[15,20,25], very thin compressible soft coatings on rigid substrates[21,26–29], and substrates of intermediate thicknesses[23,30,31] in both two- and three-dimensional settings.

A focus of previous work has been to study the relationships between sliding speeds and the resulting lift and drag forces (normal and tangential to the motion, respectively). In particular, elastohydrodynamic lift forces have been used to infer the mechanical properties of soft surfaces[14,32], sort particles and cells in microfluidics[33] and understand the radial migration of particles in blood micro-circulation[13]. By contrast, applications such as soft robotics[34], tribo-rheometry of soft surfaces[35,36] and lubrication of artificial synovial joints[37,38] have focused on drag forces in lubricated soft systems.

Recent experiments have shown that, in addition to the lift force, lubricated sliding between soft surfaces also generates an elastohydrodynamic torque[28,29]. This leads to an spontaneous rotation of a suspended cylinder sliding past a compliant substrate, at a rate that approaches its translation speed. By contrast, theoretical analyses for small deformations with both thin[39] and thick[25] elastic coatings find rotation rates that are far lower than those measured experimentally. Rotation also plays an important part of lubricated tribometric experiments[34,35] that use

[a] Department of Mechanical Engineering, University of California, Riverside, California, 92521, USA. E-mail: bhargav@engr.ucr.edu
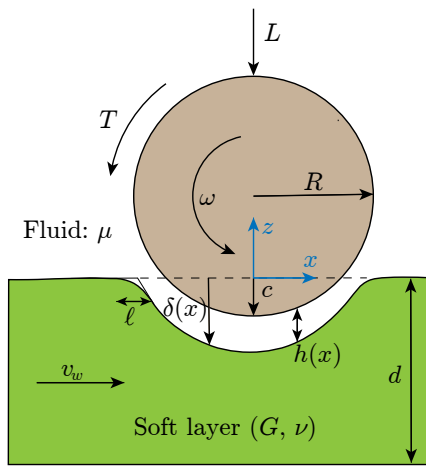
Fig. 1 Sketch of the geometry and the coordinate system for an infinite cylinder submerged in a fluid and rotating parallel to a soft moving substrate.

large normal loads, where solid deformation is large relative to the fluid film thickness and the contact is Hertzian. However, the coupling between rotation and translation, and their relation to the torque on the system, remains largely investigated outside the small-deformation (non-Hertzian) regime.

Here, by allowing for Hertzian contacts, we show that rotation and translation are very tightly coupled in soft lubricated systems. In particular, we find that rotation rate of a torque-free cylinder sliding past a soft substrate approaches its translation speed as the substrate becomes more compliant, while simultaneously recovering the results of Rallabandi *et al.*[39] for stiff substrates. We also discuss the rotation of objects subject to an applied torque and find several interesting phenomena including backspin behaviors with rotation and translation in either direction, and multiple possible states for the same torque distinguished by different fluxes through the lubricating fluid film. We understand these results using a combination of physical arguments, scaling analysis and asymptotic theory, and show that the qualitative features are robust independent of the thickness of the solid layer and the precise mode of solid deformation.

This paper is organized as follows: In Sec. 2, we set up the model governing the lubricated flow and deformation of a thick elastic solid. In Sec. 3, we discuss numerical solutions of the elastohydrodynamic problem under the specified dynamical constraints of force and torque. We show how solutions to the problem yield a relationship between rotation and translation in Sec. 4. We investigate both torque-free rotation as well as situations in which rotation is driven under a finite externally applied torque. In Sec. 5, we study the analogous problem for thin compressible coatings and find that the physical arguments that lead to translation-rotation coupling remain qualitatively unchanged, before concluding in Sec. 6.

2 Formulation

2.1 Governing equations

We consider the motion of a cylinder submerged in a fluid near a soft substrate that translates with the velocity v_w as depicted in Fig. 1. The fluid is assumed to be Newtonian with viscosity μ, and the flow is assumed to be incompressible and at steady state. We treat the soft substrate as a linearly elastic material with shear modulus G and Poisson's ratio ν. A normal force L is applied to the cylinder and keeps it near the deformable surface. Additionally, an external torque T (defined counterclockwise positive) may also be applied to the cylinder. Stresses of the flow together with the applied torque drive the cylinder to rotate with angular velocity ω, which is apriori unknown. The goal is to then relate this rotation rate to the translation speed of the surface for a specified load L and torque T.

Relative motion between the surfaces establishes a fluid film of thickness $h(x)$ between the cylinder and the elastic substrate. We assume that the cylinder radius R is considerably greater than the fluid film thickness and that the inertia of the flow is negligible. Thus, lubrication theory can be employed in the entrained fluid layer and the velocity can be written as

$$v_x = \frac{1}{2\mu}\frac{\partial p}{\partial x}(z+\delta)(z+\delta-h) + \frac{z+\delta}{h}(R\omega) + v_w\left(1 - \frac{z+\delta}{h}\right), \quad (1)$$

where $p(x)$ is the pressure, $\delta(x)$ is the surface deformation of the soft layer (defined positive when the solid is depressed) and z and x represent the normal and horizontal coordinate axes, respectively (Fig. 1). Requiring that the fluid flux remain constant at steady state leads to the Reynolds lubrication equation

$$\frac{\partial}{\partial x}\left(h^3\frac{\partial p}{\partial x} - 6\mu(v_w+R\omega)h\right) = 0. \quad (2)$$

The Reynolds equation does not depend independently on the translational or rotational velocities but only on their sum $(v_w + R\omega)$, which is often referred to as the entrainment velocity.

The film thickness $h(x)$ is a function of the cylindrical geometry as well as the surface deformation $\delta(x)$ of the elastic material. In the vicinity of the lowest point of the cylinder $(x = 0)$, we can write

$$h(x) = -c + \frac{x^2}{2R} + \delta(x), \quad (3)$$

where c is the cylinder penetration depth at $x = 0$ and is constant at a given entrainment velocity. Positive c indicates that the cylinder penetrates the undeformed nominal surface of the layer, as sketched in Fig. 1, while negative c corresponds to a finite clearance between the undeformed surfaces.

The deflection of the soft layer δ in (3) is related to the pressure p in the fluid layer via the elastic response of the soft substrate. In this paper, we discuss this response for two limiting cases, namely a thick elastic substrate and a thin compressible elastic coating. We will focus primarily on thick substrates (i.e. an elastic half-space), where the surface deformation is related to the applied pressure by an integral equation[40]

$$\delta = -\frac{1-\nu}{\pi G}\int_{-\infty}^{\infty}\ln|x-s|\,p(s)\,ds, \quad (4)$$

valid in the limit $d \gg \sqrt{|c|R}$. Note that (4) is only defined up to an arbitrary datum under two-dimensional elasticity[40]; this detail is absorbed into the definition of c in (3). The limit of a thin (and compressible) coating of thickness $d \ll \sqrt{|c|R}$ will turn out to be qualitatively (and in some limits, quantitatively) similar and will be discussed in Sec. 5.

Equations (2)–(3), subject to conditions of vanishing pressure $p(\pm\infty) = 0$, yield a coupled system for the pressure $p(x)$. However, two parameters of the problem, viz. the vertical location of the cylinder c and the rotation rate ω, remain unspecified. These are determined self-consistently so that the stresses of the flow counteract the applied normal load L and the applied torque T, necessary to keep the system in equilibrium. These conditions are written as

$$L = \int_{-\infty}^{\infty} p \, dx, \tag{5a}$$

$$T = \int_{-\infty}^{\infty} R \frac{\partial v_x}{\partial z}\bigg|_{z=-\delta+h} dx = R \int_{\infty}^{\infty} \left(\frac{h}{2} \frac{\partial p}{\partial x} - \frac{\mu}{h}(v_w - R\omega) \right) dx, \tag{5b}$$

The system (2)–(5) now simultaneously determines the pressure $p(x)$, the vertical location of the cylinder c and the angular velocity ω in terms of v_w, the applied normal load L, the applied torque T and the geometric and material properties of the system.

2.2   Non-dimensionalization

We solve a rescaled form of the governing equations. Our normalization is based on the limit of small velocities wherein, under a finite normal load L, the surfaces approach "dry" Hertzian contact[40]. In this dry limit, the surfaces make solid to solid contact over a horizontal contact length $2a$. The contact is associated with a pressure whose maximum we denote by p_{max}. Using (7), we introduce normalized quantities (indicated by overbars) as

$$\bar{x} = \frac{x}{a}, \qquad \bar{h} = \frac{h}{a^2/(2R)}, \qquad \bar{c} = \frac{c}{a^2/(2R)}, \qquad \bar{p} = \frac{p}{p_{max}}. \tag{6}$$

For thick elastic substrates $(d \gg a)$, a and p_{max} are related to the applied load L and the geometric and elastic properties of the system by[40]

$$a = \sqrt{\frac{2(1-\nu)}{\pi G} RL}, \quad p_{max} = \frac{2L}{\pi a}. \tag{7}$$

Defining a normalized sliding velocity λ and a normalized rotational velocity Ω by

$$\lambda = \frac{6\pi^2 \mu GR v_w}{(1-\nu)L^2} \quad \text{and} \quad \Omega = \frac{6\pi^2 \mu GR^2 \omega}{(1-\nu)L^2}, \tag{8}$$

and a normalized entrainment velocity

$$\Lambda = \lambda + \Omega = \frac{6\pi^2 \mu GR}{(1-\nu)L^2}(v_w + R\omega), \tag{9}$$

the governing equations (2)–(4) rescale as

$$\frac{\partial}{\partial \bar{x}} \left(\bar{h}^3 \frac{\partial \bar{p}}{\partial \bar{x}} - \Lambda \bar{h} \right) = 0, \tag{10a}$$

$$\bar{h} = -\bar{c} + \bar{x}^2 - \frac{2}{\pi} \int_{-\infty}^{\infty} \ln|\bar{x} - \bar{s}| \, p(\bar{s}) \, d\bar{s}, \tag{10b}$$

subject to boundary conditions $\bar{p}(\pm\infty) = 0$. The condition of normal force balance (5a) rescales as

$$\int_{-\infty}^{\infty} \bar{p} \, d\bar{x} = \frac{\pi}{2}. \tag{11}$$

The entrainment velocity Λ can alternatively be interpreted as a dimensionless compliance: small Λ correspond to soft substrates (small shear modulus G), whereas large Λ occur for relatively stiff substrates.

Observe that the (10a) and (10b) form a complete system in terms of the sole parameter Λ (the normalized entrainment velocity) but do not depend individually on λ and Ω. The solution of this system thus yields $\bar{p}(x)$, $\bar{h}(x)$ and $\bar{c}$ in terms of Λ, which we detail in the forthcoming Sec. 3. The relation between Ω and λ is determined by the torque condition (5b), which we discuss and enforce subsequently in Sec. 4.

3   Solution of the elasto-hydrodynamic problem

We first present numerical solutions of the system of constrained integro-differential equations (10) and (11) over the entire range of Λ, and interpret the results with asymptotic arguments. The limit of $\Lambda \ll 1$ was analyzed by Bissett and Spence[16], Wu et al.[19], Snoeijer et al.[20], Bissett[41] and the limit $\Lambda \gg 1$, by Zhang et al.[15], Skotheim and Mahadevan[23], Bertin et al.[25], Kargar-Estahbanati and Rallabandi[31], albeit using a different formulation (see appendix). Our numerical results span the entire range of Λ and are consistent with either limit. Recently, Essink et al.[21] simulated the entire range of Λ using both lubrication theory and finite element analysis, focusing on thin elastic coatings (we return to thin coatings in Sec. 5). Below, we summarize the main features of the flow for thick substrates, focusing on the cylinder's vertical location $\bar{c}$, the pressure $\bar{p}$ and the film thickness profiles $\bar{h}$ as functions of Λ. These results are necessary for understanding the coupling between rotation and translation, which we discuss later.

At each Λ, we solve the system of equations by first guessing a $\bar{c}$. We cast the derivatives in (10a) and integral in (10b) as matrix-vector products using finite-difference approximations, with an analytic treatment of the integral in (10b) near the singularity. We solve the resulting system of nonlinear algebraic equations using Newton–Raphson iteration. While the obtained numerical solution solves the flow equations (10), it does not satisfy (11) needed to ensure the balance of normal forces. Thus, we iterate on $\bar{c}$ until the integral condition (11) is met within a small tolerance, yielding the solution to the problem. For $\Lambda \ll 1$, we use a non-uniform mesh to resolve the problem efficiently around the contact lines $\bar{x} = \pm 1$ while maintaining accuracy.

Fig. 2 shows $\bar{c}$ as a function of entrainment velocity Λ. As de-
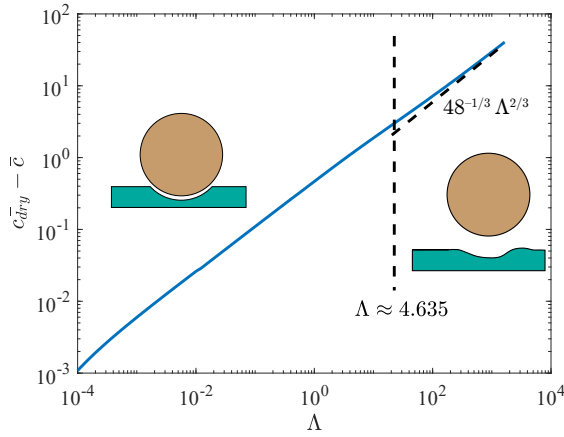
Fig. 2 Normalized indentation of bottom of cylinder $\bar{c}$ as a function of Λ (normalized entrainment velocity). The illustrations show the configuration of cylinder and soft surface in the limiting cases, qualitatively. The indentation in the limit $\Lambda \to 0$ is $\bar{c}_{dry} = \frac{1}{2}(1 + 2\log 2)$. The vertical dashed line at $\Lambda = 4.635$ is the location where $\bar{c}$ crosses over from positive to negative values.

picted in Fig. 1, $\bar{c}$ is the normalized penetration depth at $x = 0$ and is constant for a given Λ. In the (singular) limit of vanishingly small speeds ($\Lambda \to 0$), the solution approaches that of dry contact and the parameter $\bar{c}$ is found analytically to equal $\bar{c}_{dry} = \frac{1}{2}(1 + 2\log 2) \approx 1.1931$; Fig. 2. As Λ is increased, the thickness of entrained fluid film increases and the deformation of soft layer decreases thus $\bar{c} = \bar{\delta}(0) - \bar{h}(0)$ decreases. At $\Lambda \approx 4.635$, $\bar{c} = 0$ which corresponds to the region where the cylinder starts to "float" above the undeformed surface. Further increasing Λ increases the separation between the surfaces (so $\bar{c}$ becomes negative). In the limit where $\Lambda \gg 1$, Skotheim and Mahadevan[23] provided an analytical solution, which in our normalization yields $\bar{c} = -48^{-1/3}\Lambda^{2/3}$ (details in the appendix). This result (dashed line in Fig. 2) is in good agreement with numerical results in this limit.

Dimensionless fluid pressure $\bar{p}(\bar{x})$ and thickness $\bar{h}(\bar{x})$ profiles are plotted in Figs. 3a and 3b, respectively; the arrow shows the direction of increase in Λ. The lubrication pressure decays away from the cylinder as required by the boundary conditions. For small entrainment speeds ($\Lambda \ll 1$), the cylinder is pushed into the surface, squeezing out most of the fluid except for a very thin entrained layer. In this case, the pressure distribution approaches that of dry contact in most of the domain, $\bar{p} \sim \sqrt{1 - \bar{x}^2}\,\Theta(1 - \bar{x}^2)$ up to corrections involving Λ, with Θ denoting the Heaviside function. However, near the nominal contact lines ($\bar{x} \sim \pm 1$), the presence of the thin fluid layer smooths the originally sharp pressure gradients of dry contacts. This smoothing occurs over two regions of dimensional width ℓ around the contact lines (Fig. 1, Fig. 3). Asymptotic theory[20] shows that the width of the boundary layer scales as $\ell \sim a\Lambda^{2/5}$. As noted earlier, as Λ increases, there is a greater flux of fluid through the gap, increasing the gap width, leading to smaller pressures and smaller surface deformations. For small Λ, the fluid film thickness $\bar{h} = H^*\Lambda^{3/5}$ (with $H^* = 0.389$) is asymptotically constant throughout the nominal contact region
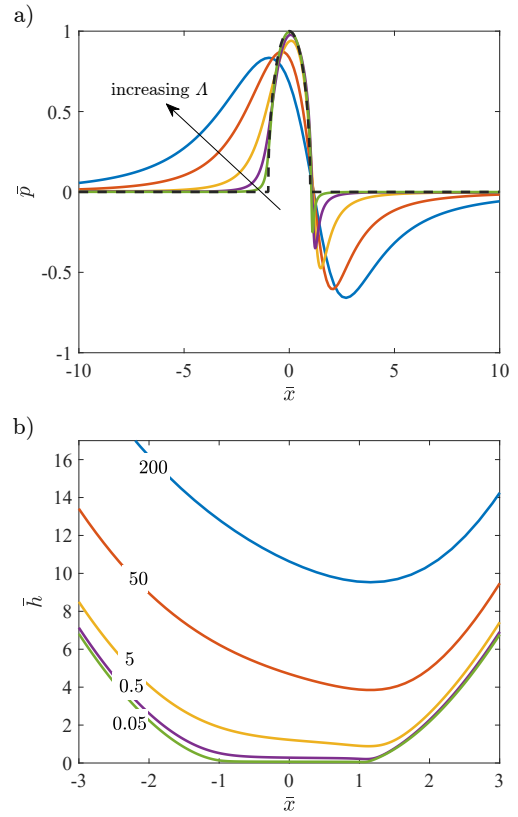

Fig. 3 a) Normalized pressure and b) normalized fluid thickness as a function of horizontal coordinate $\bar{x}$ for different values of normalized entrainment velocity. $\Lambda = 0.05, 0.5, 5, 50, 200$. The arrow shows the direction of increase in Λ. The dashed line corresponds to the pressure distribution of dry contact.

($-1 < \bar{x} < 1$), consistent with analysis of Snoeijer *et al.*[20].

At the other extreme of large Λ, the cylinder floats far above the surface ($\bar{h} \gg \bar{\delta}$), and the pressure approaches the pure hydrodynamic solution for the motion of a rigid cylinder parallel to a rigid wall in a viscous fluid, plus small corrections due to the compliance of the substrate. In this limit, our numerical results are consistent with the analysis of Skotheim and Mahadevan[23] (the limit $\eta \ll 1$ in that article).

We observe that both the pressure and film thickness profiles depend on $\Lambda = \lambda + \omega$, so at this stage it is not yet clear how rotation and translation are coupled. In subsequent sections, we show how the dynamical constraints on the applied torque relates translation and rotation.

4 Coupling between translation and rotation

Having solved the lubrication equations in terms of $\Lambda = \lambda + \Omega$, we are now in a position to relate Ω to λ using the torque balance (5b). Using (5) the normalized torque on the cylinder is

$$\bar{T} = \frac{T}{La} = \frac{1}{2\pi}\left(A - \frac{1}{3}\frac{\Lambda - 2\Omega}{\Lambda}B\right), \qquad \text{where} \qquad (12a)$$

$$A(\Lambda) = \int_{-\infty}^{\infty}\bar{h}\frac{\partial\bar{p}}{\partial\bar{x}}d\bar{x} \qquad \text{and} \qquad B(\Lambda) = \int_{-\infty}^{\infty}\Lambda\frac{d\bar{x}}{\bar{h}}. \qquad (12b)$$
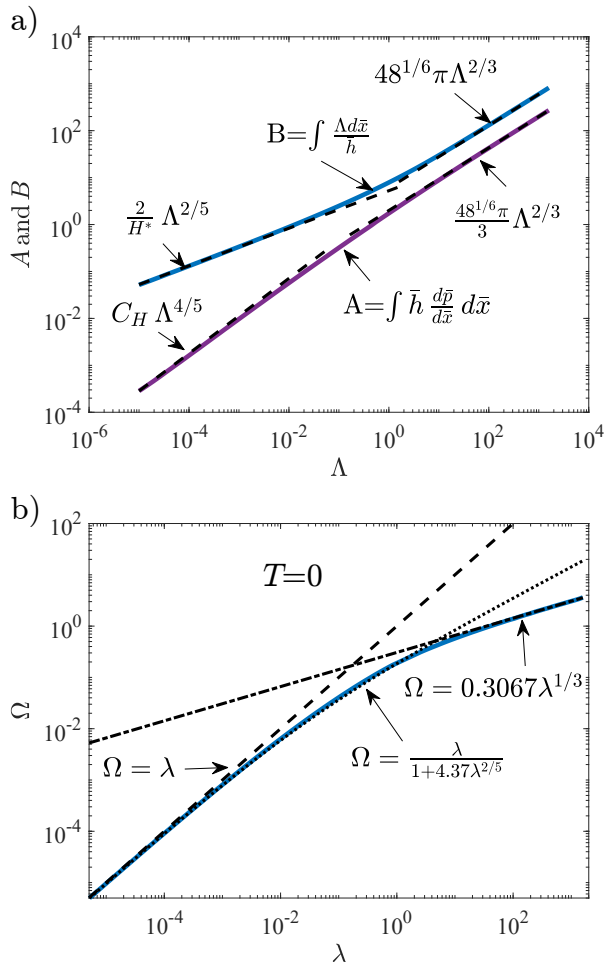
Fig. 4 a) A and B for the different values of normalized entrainment velocity. b) Normalized rotational velocity vs normalized sliding velocity for the torque free problem. The solid lines represent the numerical solution and the dashed lines are asymptotic solutions.

The integrals A and B depend solely on Λ and are obtained using the numerical solutions for $\bar{h}$ and $\bar{p}$ discussed in Sec. 3. In (12a), the term involving A represents the contribution of Poiseuille flow whereas the term involving B is due to the effect of simple shear in the gap.

Rearranging (12a) yields Ω as a function of Λ and the integrals $A(\Lambda)$ and $B(\Lambda)$ as

$$\Omega = \frac{\Lambda}{2}\left(1 - \frac{3A - 6\pi\bar{T}}{B}\right). \tag{13}$$

Since $A(\Lambda)$ and $B(\Lambda)$ in (12b) are essential in understanding the mechanism of rotation, we will first discuss their behaviour in detail. Once we find A and B, the relation between Λ and Ω is a rational function (13).

Fig. 4a shows plots of $A(\Lambda)$ and $B(\Lambda)$ for thick elastic layers, obtained from the numerical solutions of Sec. 3. For small Λ, the dominant contribution to A comes from the boundary layers around the contact lines $x \sim \pm 1$, where $\bar{h} = O(\Lambda^{3/5})$ and $\mathrm{d}\bar{p}/\mathrm{d}\bar{x} = O(\Lambda^{-1/5})$ yielding $A \sim C_H \Lambda^{4/5}$. The prefactor $C_H \approx 2.84$ is obtained numerically. The primary contribution to B comes from the

contact region, where the film thickness is a constant ($h \sim H^* \Lambda^{3/5}$) yielding $B = 2\Lambda^{2/5}/H^*$. Similarly, for large Λ, $\bar{p} = O(1)$ because of the constraint imposed by (11), $\bar{h} \sim c \sim \Lambda^{2/3}$ and the horizontal length scale $\sqrt{|c|} \sim \Lambda^{1/3}$, yielding $A \sim \Lambda^{2/3}$ and $B \sim \Lambda^{2/3}$. For both small and large Λ our numerical results approach the above asymptotic relations (details are in the appendix). We are now in a position to use the results for $A(\Lambda)$ and $B(\Lambda)$ in (13) to relate the rotation rate Ω to the translation speed $\lambda = \Lambda - \Omega$.

4.1 Free rotation ($\bar{T} = 0$)

We first discuss the case where no external torque is applied ($\bar{T} = 0$), so the cylinder rotates freely. Fig. 4b shows the plot of Ω for the different values of λ when $\bar{T} = 0$. For small sliding velocities, $\Omega \sim \lambda$, or $R\omega \sim v_w$, represented by a dashed line in Fig. 4b. This asymptotic result follows from (13) as $A \ll B$ (see Fig. (4a)) and represents "pure rolling", which occurs in the limit of small velocities or highly compliant substrates (at fixed normal load). Physically, the thin layer of entrained fluid has constant thickness ($\Lambda^{3/5} H^*$), so hydrodynamic torque is generated essentially by shear stress across the fluid film due to the relative velocity $\lambda - \Omega$. Therefore, for the system to be torque free, it is necessary for the rotational speed of the cylinder to match its sliding speed.

An improved approximation for Ω retaining higher-order terms (see appendix) in the behaviors of A and B. We use these terms to construct a Padé approximant $\Omega = \lambda/(1 + 4.37\lambda^{2/5})$ that is asymptotic for small λ, but has excellent accuracy up to $\lambda \simeq 4$ (Fig. 4b; dotted curve). We note that the rotation speed becomes comparable to the translation speed for compliant surfaces (small λ). This result is in qualitative agreement with the experiments of Saintyves et al. [29] which found rotation rates as large as $R\Omega/v_w \approx 0.7$ and where it was observed that softer substrates led to faster rotation.

For large speeds or stiff substrates ($\lambda \gg 1$) the pressure amplitude is $O(1)$, leading to a deformation scale $\lambda^{1/3}$, while the film thickness grows as $\lambda^{2/3}$. The ratio of deformation to film thickness thus scales as $\delta/h \propto \lambda^{-1/3} \ll 1$, as discussed in the appendix in detail. For thin compressible elastic substrates, Rallabandi et al. [39] showed that $\Omega/\lambda \propto (\delta/h)^2$, and rationalized the scaling behavior through symmetry arguments. We expect the same symmetry arguments to apply for thick elastic substrates, and thus we anticipate $\Omega/\lambda \propto \lambda^{-2/3}$, or $\Omega \propto \lambda^{1/3}$. This scaling estimate is borne out by numerical solutions, which we use to make the scaling law more precise as $\Omega \sim 0.307\lambda^{1/3}$; cf. Fig.4b. Thus, the combination of scaling arguments, asymptotic estimates and numerical solutions provide handy approximations to Ω over the entire range of λ for a torque-free cylinder.

4.2 Rotation at finite torque ($\bar{T} \neq 0$)

While we have so far considered rotation of torque-free cylinders, several applications rely on the application of a finite torque. For example, a Mini-traction machine, a tribometric apparatus designed to measure the frictional force in soft contacts, keeps the probe from rotating ($\Omega = 0$) by applying a finite external torque $\bar{T}$ [34–36]. The response to applied torques is also relevant in the study of natural or artificial lubricated joints involving soft
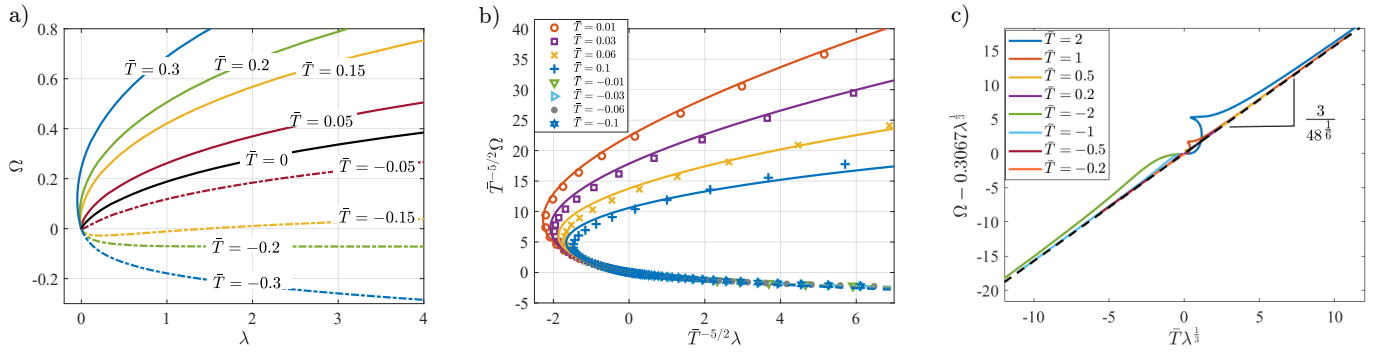
Fig. 5 a) Normalized rotational velocity Ω vs normalized sliding velocity λ for $\bar{T} = 0, \pm 0.05, \pm 0.15, \pm 0.2, \pm 0.3$. The dashed lines represents negative torques. b) Rescaled curves for different torques showing an approximate collapse when $\lambda, \Omega \ll 1$. The lines represent analytical solutions (solid lines for $T > 0$ and dashed lines for $T < 0$) and the symbols represent numerical solutions. c) large λ approximation for different applied torques. The solid lines are numerical solutions while the dashed line is an analytic result.

tissue [37,38]. Therefore, we now return to (13) and discuss the rotation-translation coupling under the application of an external torque to the cylinder. The torque applied may either be positive (counter clockwise) which aids rotation, or negative (clockwise) which opposes it.

Figure 5a plots Ω vs λ for different values of the normalized externally applied torque $\bar{T}$, obtained by substituting the numerical values of the integrals A and B into (13). As shown in Fig. 5a, for a given translation velocity λ, the cylinder is able to spin backward (clockwise), forward (counter-clockwise) or translate without any rotation, depending on the magnitude and direction of the external torque. Unsurprisingly, positive $\bar{T}$ result in larger rotation rates than the torque-free cases, whereas negative $\bar{T}$ yields lower rotation rates, ultimately producing a reversal of the direction of rotation. However, it is interesting to note that positive $\bar{T}$ yields solutions with where the direction of *translation* is reversed ($\lambda < 0$), leading to multiple Ω at the same (negative) λ for positive $\bar{T}$ (see also Fig. 5b). Similarly, the direction of rotation may depend on the translation speed λ at some negative values of $\bar{T}$ (e.g., the curve for $\bar{T} = -0.15$ in Fig. 5a crosses the $\Omega = 0$ axis). Similar to the torque-free case, we use the asymptotics of A and B to quantify these behaviors.

Substituting the asymptotic relations for A and B for $\lambda \ll 1$ and $T \ll 1$ into (13), the relation between rotational and sliding velocity becomes $\Omega \sim \lambda + 3\pi H^* \bar{T}(\lambda + \Omega)^{3/5} - 3/2\, H^* C_h(\lambda + \Omega)^{7/5}$ (details in appendix). A dominant balance for small λ and Ω suggest the rescaling $\hat{\Omega} = \Omega/|\bar{T}|^{5/2}$, and $\hat{\lambda} = \lambda/|\bar{T}|^{5/2}$, yielding

$$\hat{\Omega} \sim \hat{\lambda} + \text{sgn}(\bar{T})3\pi H^*(\hat{\lambda} + \hat{\Omega})^{\frac{3}{5}} - \frac{3}{2}H^* C_h(\hat{\lambda} + \hat{\Omega})^{\frac{7}{5}}|\bar{T}| \qquad (14)$$

where sgn is the sign function. In these new rescaled coordinates, the leading terms are independent of T, whereas the effect of finite T occurs in a higher-order term. Indeed, numerical results of Fig. 5a when suitably rescaled are well predicted by (14), as illustrated for different values of external torque in Fig. 5b. The numerical results start to deviate from this relation for large λ or large $|\bar{T}|$. As one can observe in Fig.5b, when the external torque is applied in the "natural" direction of rotation ($\bar{T} > 0$), there are some conditions wherein the cylinder translates with a backspin ($\lambda < 0$, and $\Omega > 0$, but with $\Lambda = \lambda + \Omega > 0$). This non-

trivial behavior can also be observed in Fig. 5a and is not limited to small torques. The analytical solution (14) provides insight into this "turn-over" region of the curves for positive torques: for example, for an applied positive $\bar{T} \ll 1$, the maximum value of negative translation speed that can be attained is $\lambda \approx 2.2\bar{T}^{5/2}$.

Furthermore, for a prescribed external torque, there are two equilibrium Ω for each (negative) value of λ in the backspin region. As a case in point, solving (14) for zero linear velocity and $\bar{T} \ll 1$ yields: $\Omega = 0$ and $\Omega \approx (3\pi H^*)^{5/2}\, T^{5/2}$. The first solution represents the static condition where the objects move at vanishingly small speeds. The second solution, however, corresponds to rotation in place without translation.

Whether one solution or another is selected depends on other constraints of the system. In particular, the external horizontal force $\bar{D}$ on the cylinder must also be supported by fluid stresses, so that

$$\bar{D} = \frac{D}{L} = \frac{1}{2\pi}\left(E + \frac{1}{4}A - \frac{1}{12}\frac{\Lambda - 2\Omega}{\Lambda}B\right), \qquad (15a)$$

$$\text{where} \qquad E(\Lambda) = \int_{-\infty}^{\infty} \bar{x}\bar{p}\,d\bar{x}. \qquad (15b)$$

While the multiplicity of solutions pointed out earlier have the same normal load and torque, they correspond to different values of Λ and thus are require different horizontal forces to sustain.

Similarly, for external torques that are applied clockwise in Fig. 1 ($\bar{T} < 0$), we again find situations in which the cylinder translates with a backspin, but this time with $\Omega < 0$ while maintaining $\lambda > 0$ (still with $\Lambda = \lambda + \Omega > 0$). In analogy to the case of $\bar{T} > 0$, there are two possible λ corresponding to the same (negative) Ω within this backspin region. For small $\bar{T} < 0$, this region of negative Ω ultimately yields to positive Ω for large enough λ due to the translation-rotation coupling overwhelming the counteracting negative torque. However, for sufficiently negative T, this behavior disappears and the applied torque is able to support a backspin at equilibrium for all λ.

For large translation speeds $\lambda \gg 1$, we find from (13), using the asymptotic behaviors of A and B (Fig. 4a) that (see appendix)

$$\Omega = 0.307\lambda^{\frac{1}{3}} + \frac{3}{48^{\frac{1}{6}}}\bar{T}\lambda^{\frac{1}{3}}. \qquad (16)$$

Figure 5c shows that the above relation is in excellent agreement with the numerical results for different values of external torque for large λ. The result (16) also identifies the smallest negative torque required to produce backspin ($\Omega < 0$) for all $\lambda > 0$, viz. $\bar{T}_{min}^{back} \approx -0.195$. This estimate is borne out by our numerical solutions, though we do not display this in Fig. 5.

5 Thin elastic coating

Many applications utilize thin elastic coatings on rigid substrates[28,29]. We show that our discussion for thick elastic susbtrates remains qualitatively unchanged when the thickness of the soft coating is much smaller than the horizontal length scale of the problem ($d \ll a$). We will reuse notation from our analysis of thick substrates for convenience. Assuming that the solid is not strictly incompressible ($\nu \neq 1/2$), the relation between pressure and deformation in this limit is local (the Winkler approximation) and given by $\delta = pd(1-2\nu)/(2G(1-\nu))$. Analogously to Sec. 2.2 we define the dry contact length and the maximum dry contact pressure for thin elastic layers as[21]

$$a = \left(\frac{3}{4} \frac{LdR(1-2\nu)}{G(1-\nu)} \right)^{\frac{1}{3}}, \quad p_{max} = \frac{3L}{4a}. \tag{17a}$$

The governing equation in the fluid film is still (10a). For thin substrates, the normalized rotational and translational velocities are

$$\lambda = 32 \frac{v_w \mu R^2}{La^2} \quad \text{and} \quad \Omega = 32 \frac{\omega \mu R^3}{La^2}. \tag{18}$$

In dimensionless variables, the relation between deformation and pressure is simplified to $\bar{p} = \bar{\delta}$ and therefore, we write the normalized film thickness $\bar{h}$ as

$$\bar{h} = \bar{x}^2 - \bar{c} + \bar{p}. \tag{19}$$

Additionally, the equilibrium of normal forces (5a) and external torques (5b) for thin layers rescale as

$$\int_{-\infty}^{\infty} \bar{p}\, d\bar{x} = \frac{4}{3}, \tag{20a}$$

$$\bar{T} = \frac{T}{La} = \frac{3}{16} \left(A - \frac{\Lambda - 2\Omega}{3\Lambda} B \right). \tag{20b}$$

We use a similar approach as that for thick layers to find the pressure $\bar{p}(x; \Lambda)$ and film thickness $\bar{h}(x; \Lambda)$ for different values of entrainment velocity. Here, we use solve the governing equation using a shooting method instead of Newton–Raphson iteration. Once the solution is obtained, rearranging (20b) yields Ω as

$$\Omega = \frac{\Lambda}{2} \left(1 - \frac{3A - 16\bar{T}}{B} \right) \tag{21}$$

Equations (20b) and (21) differ from their thick-layer counterparts (12a) and (13) only by a numerical factor.

As depicted in Fig. 6 a, for $\Lambda \ll 1$, both A and B decay like $\Lambda^{1/2}$. This is due to the feature that the fluid film is not uniform in this limit for thin elastic layers[21], contrary to the case of thick layers[20]. Both A and B are therefore involved in the calculation of Ω at leading order. As a result, in the limit of soft coatings, the
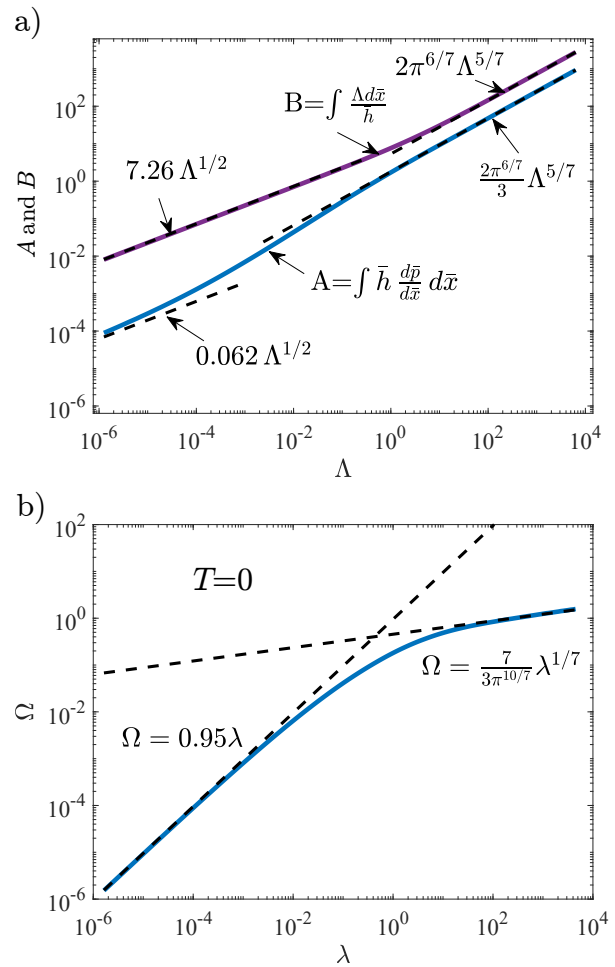

Fig. 6 a) A and B as a function of normalized mean velocity Λ, and b) Ω as a function of normalized linear velocity λ, for thin elastic layers and zero applied torque. Dashed lines represent the asymptotic solutions.

ratio of rotational to linear velocity Ω/λ does not approach unity as $\Lambda \to 0$. Nonetheless, if we substitute the asymptotic values for A and B in (21), we find $\Omega \sim 0.95\lambda$, which remains very close to pure rolling. This asymptotic result is illustrated in Fig. 6b. All indicated asymptotes in Fig. 6a and Fig. 6b are derived analytically including the prefactors (see appendix). As noted above, the fluid film thickness for a thin elastic coating is not uniform for $\Lambda \ll 1$. The hydrodynamic torque thus has two contributions, one scaling as $\lambda - \Omega$, and the other depending on the pressure gradient; both are involved in the zero-torque condition.

At the other extreme, where $\Lambda \gg 1$, analytical solutions are found using the asymptotic analysis of Skotheim and Mahadevan[26]. The quantities A and B are qualitatively similar to their counterparts for thick substrates. Additionally, as depicted in Fig. 6 b, $\Omega = 7/\left(3\pi^{10/7}\right) \lambda^{1/7}$, in agreement with the analytical result of Rallabandi et al.[39] (see appendix).

By comparing Fig. 4b and 6b, we see that behaviour of the Ω versus λ curve is qualitatively the same for the limiting cases of thick ($d \gg a$) and thin (compressible) elastic layers ($d \ll a$, $\nu \neq 1/2$). Some important asymptotic behaviors for the rotation-translation coupling with thick and thin elastic substrates are

Table 1 Relation between normalized linear velocity λ and normalized rotational velocity Ω for the extreme conditions. $\lambda = 24k_c v_w \mu R^2/(La^2)$ and $\Omega = 24k_c \Omega \mu R^3/(La^2)$ where $k_c = \pi/2$ for thick layers and $k_c = 4/3$ for thin layers.

	horizontal length scale	large deformation $\Lambda \ll 1$	small deformation $\Lambda \gg 1$
thick layers $d \gg a$	$a = \sqrt{\dfrac{2(1-\nu)}{\pi G} RL}$	$\Omega - \lambda - 3\pi H^*(\lambda + \Omega)^{3/5} \bar{T} - 3/2 H^* C_h (\lambda + \Omega)^{7/5} = 0$	$\Omega = \lambda^{1/3}\left(0.307 + \dfrac{3\bar{T}}{48^{1/6}}\right)$
thin layers $d \ll a$	$a = \left(\dfrac{3}{4}\dfrac{LdR(1-2\nu)}{G(1-\nu)}\right)^{1/3}$	$\Omega - 0.95\lambda - 2.15(\lambda + \Omega)^{1/2}\bar{T} = 0$	$\Omega = \dfrac{7}{3\pi^{10/7}}\lambda^{1/7} + \dfrac{4\bar{T}}{\pi^{6/7}}\lambda^{2/7}$

summarized in Table 1. We note that the thin-layer theory used here assumes that the elastic layer is thinner than all lateral length scales, in particular also that of the boundary layer, whose width scales as $\ell \sim a\Lambda^{1/2}$. This condition can no longer be met at sufficiently small speeds $\Lambda \lesssim (d/a)^2$, where it becomes necessary to account for the full (finite-thickness) response of the layer, leading to new asymptotics as $\Lambda \to 0$ (see Essink *et al.* [21]). We do not anticipate these effects to significantly affect our results for rotation in this limit, since the bulk of the rotation is caused by stresses in the thin film (and not the boundary layers) which remains well approximated by the local elastic model used here as long as $d \ll a$. More generally, the finite-thickness elastic response is necessary everywhere if d is comparable to a. However, due the observed similarities for the limiting cases of thick and thin elastic layers, we anticipate that the rotation behaviors discussed here are qualitatively robust even for soft layers of intermediate thickness.

6 Conclusions

In this paper, we investigated the coupling of rotation and translation in the lubricated motion of soft objects. For compliant substrates, there is a strong coupling between the rotation and translation, approaching the limit of classical frictional rolling for highly compliant materials ($R\omega \simeq v_w$). This coupling is significantly stronger than was predicted by previous approaches, which focused on relatively stiff substrates. When the surfaces are relatively stiff, translation and rotation remain coupled but to a lesser extent ($R\omega \propto v_w^{1/3}$). The behavior of soft contacts are found to be quantitatively similar for thin and thick soft layers; some key quantitative results are summarized in Table 1. Finally, we showed that applying an external torque in either direction modifies this coupling, yielding various combinations of translation and rotation depending on the magnitude and direction of the applied torque. In particular, this includes back-spinning behavior with translation and rotation in either direction, as well as multiple possible states for the same applied torque but with differing fluxes. These behaviors could have implications for the tribology of soft surfaces and may lead to new ways to control motion in systems such as artificial joints that involve lubricated soft materials.

Author Contributions

A. K.-E. developed the theory and simulations. Both authors conceived the project, analyzed the results and and wrote the paper.

Conflicts of interest

The authors have no conflicts of interest.

Acknowledgements

A Asymptotic analysis for compliant and stiff substrates

A.1 Analysis for $\Lambda \gg 1$

In this section, we establish a relation between the normalization of previous works in the limit of large sliding velocity ([23,24,26,39]) and the normalization we use here. We employ the results of this section to compare our numerical results with asymptotic solutions.

In Skotheim and Mahadevan [23] the normalized relation for the fluid thickness and the lubrication equation are written as

$$G = 1 + Z^2 + \eta \int Q(r)\ln|Z - r|\,dr, \tag{22a}$$

$$\frac{dQ}{dZ} = 6\frac{G - G^*}{G^3}, \tag{22b}$$

where G and Q are the normalized thickness and pressure, respectively, Z is the rescaled horizontal coordinate and η is a deformation parameter.

Comparing (22a) and (22b) with (10b) and (10a), we find that $\bar{x} = \sqrt{|c|}Z$, $\bar{p} = \Lambda/(6|c|^{3/2})Q$ and $\bar{h} = |c|G$; recall that $c < 0$ for $\Lambda \gg 1$. Substituting back these values in (22a), we find $\eta \sim \frac{\Lambda}{3|c|^2}$. Additionally, we know from the literature that for a very thick soft layer $\int Q\,dZ \sim \eta\frac{3\pi}{16}$ [23]. On the other hand, (11) requires that $\int \bar{p}\,d\bar{x} = \pi/2$. By substituting $\bar{p}$ and $\bar{x}$ into the latter integral, we find c as a function of Λ

$$c \sim -48^{-1/3}\Lambda^{\frac{2}{3}}. \tag{23}$$

Now, we can substitute (23) and the values of $\bar{x}$ and $\bar{p}$ into the integral relations for A and B (12b) and find these two integrals using the analytical solutions for the pressure (Q) and film thickness thickness (G). Skotheim and Mahadevan [23] show that $Q = \frac{2Z}{(1+Z^2)^2} + O(\eta)$ and $G = 1 + Z^2 + O(\eta)$, using which we find

that

$$A \sim \frac{48^{1/6}}{3}\pi\Lambda^{2/3}, \tag{24a}$$

$$B \sim 48^{1/6}\pi\Lambda^{2/3}. \tag{24b}$$

We used these values in Fig.4a in the main text to verify our numerical results in the extreme limit of $\Lambda \gg 1$. To estimate Ω using (13), higher order terms in A and B are required. However, based on the analysis in Rallabandi *et al.* [39], we expect $\Omega/\Lambda \sim \eta^2$ when no external torque is exerted on the cylinder due to symmetry arguments. Substituting (23) in the definition of η noted earlier yields $\eta \sim \Lambda^{-1/3}$. Combining these two equation, we find that Ω scales as

$$\Omega \propto \Lambda^{2/3} \propto \lambda^{2/3}. \tag{25}$$

In the main text, we use our numerical solution to fit a prefactor to the scaling law above. For finite torque, we use the torque-free result for Ω and the solutions for A and B from (24) to obtain (16) of the main text.

For thin layers [22], instead of (22a), the thickness is related to the pressure by $G = 1 + Z^2 + \eta Q(r)$. However, the lubrication equation (22b) is still valid and one can use similar approach as the one discussed above for thick layers to find asymptotic relations for the two integrals A and B. These results are depicted in Fig. 6. For thin layers, the analytical relation between Ω and λ for $\lambda \gg 1$ is known [39] to be $\Omega/\lambda = 21\eta^2/256$ (η is defined differently for thin and thick layers but we reuse notation). Our analysis finds $\eta = 16\Lambda^{3/7}/(3\pi^{5/7})$, which use to relate Ω and λ as

$$\Omega = \frac{7}{3\pi^{10/7}}\lambda^{1/7}. \tag{26}$$

This relation is compared with the numerical results for large sliding velocities in Fig. 6 b. Similarly, the finite torque relations in this limit can be found using the approach we adopted for (16).

A.2 Analysis for $\Lambda \ll 1$

For $\Lambda \ll 1$, the contact region is divided into a central region which resembles Hertzian contact, and boundary layer regions where the thin film adjusts to the flow far from contact (See details in [20,21]). In this section, we use the analytical results found in Snoeijer *et al.* [20] to approximate the scaling of integrals A and B when the entrainment velocity Λ is small. In the central region, we can approximate pressure by that of dry contact: $\bar{p} = \sqrt{1 - \bar{x}^2}\Theta(1 - x^2)$ where Θ is the Heaviside function. Additionally, (10) yields $\bar{h} = \Lambda^{3/5}H^* + \Lambda^{4/5}H^{*3}\,d\bar{p}/d\bar{x}$ where $H^* = 0.389$ is a constant. Substituting $\bar{h}$ and $\bar{p}$ back into (12b), one finds the values of A and B in central region (A_c and B_c, respectively) to be equal to

$$B_c = \frac{2}{H^*}\Lambda^{2/5}, \tag{27a}$$

$$A_c = \Lambda^{4/5}H^{*3}\int_{-1}^{1}\left(\frac{d\bar{p}}{d\bar{x}}\right)^2 d\bar{x} \sim O(\Lambda^{4/5}), \tag{27b}$$

In the boundary layers around $\bar{x} \pm 1$, $\bar{p} = \Lambda^{1/5}P(\xi)$ and $\bar{h} = \Lambda^{3/5}H(\xi)$ where $\xi = \Lambda^{-2/5}(\bar{x} \mp 1)$ is a rescaled horizontal coordinate. The contributions of the boundary layers to A and B are therefore

$$B_{bl} = \Lambda^{4/5}\int_0^\infty \frac{d\xi}{H} \sim O(\Lambda^{4/5}), \tag{28a}$$

$$A_{bl} = \Lambda^{\frac{4}{5}}\int_0^\infty H\frac{dP}{d\xi}d\xi \sim O(\Lambda^{4/5}). \tag{28b}$$

Now, the integrals A and B over the entire domain are simply the sums of contributions from the central region (27) and the two boundary layers (28), so

$$B \sim \frac{2}{H^*}\Lambda^{2/5} + B_h\Lambda^{4/5}, \tag{29a}$$

$$A \sim C_h\Lambda^{4/5}, \tag{29b}$$

We used our numerical results to find the prefactors $B_h = 3.30$ and $C_h = 2.84$. The analytical results (29) are plotted along with the numerical results in Fig. 4a. Substituting A and B from (29) back into (13), we find $\Omega = \lambda$ at the leading order when $\Lambda \ll 1$. Retaining the higher order terms gives us even a more precise expression $\Omega = \lambda - 4.37\lambda^{7/5}$. We use a Padé approximation to rewrite this relation as (see, e.g., Bender and Orszag [42])

$$\Omega = \frac{\lambda}{1 + 4.37\lambda^{2/5}}, \tag{30}$$

which is an excellent approximation up to $\lambda \approx 4$; Fig. 4b.

When a nonzero torque is applied to the cylinder, we use (29) to rewrite the rotation rate equation (13) as

$$\Omega = \frac{\Lambda}{2} + \frac{3\pi}{2}H^*\bar{T}\Lambda^{3/5} - \frac{3}{4}H^*C_h\Lambda^{7/5}. \tag{31}$$

Substituting $\Lambda = \lambda + \Omega$ yields (14).

Notes and references

1 J. Frene, D. Nicolas, B. Degueurce, D. Berthe and M. Godet, *Hydrodynamic lubrication: bearings and thrust bearings*, Elsevier, 1997.

2 E. Okrent, *ASLE Transactions*, 1961, **4**, 97–108.

3 S. Tzeng and E. Saibel, *ASLE Transactions*, 1967, **10**, 334–348.

4 J. A. McGeehan, *SAE Transactions*, 1978, 2619–2638.

5 L. Martz, *Proceedings of the Institution of Mechanical Engineers*, 1949, **161**, 1–9.

6 J. Hou, V. C. Mow, W. Lai and M. Holmes, *Journal of Biomechanics*, 1992, **25**, 247–259.

7 T. W. Secomb, R. Skalak, N. Özkaya and J. Gross, *Journal of Fluid Mechanics*, 1986, **163**, 405–423.

8 J. Bradfield, *Journal of Experimental Biology*, 1951, **28**, 125–140.

9 M. E. Rosti, M. N. Ardekani and L. Brandt, *Physical Review Fluids*, 2019, **4**, 062301.

10 B. Rallabandi, N. Oppenheimer, M. Y. B. Zion and H. A. Stone, *Nature Physics*, 2018, **14**, 1211–1215.

11 R. Gohar and A. Cameron, *Nature*, 1963, **200**, 458–459.

12 P. Cann, H. Spikes and J. Hutchinson, *Tribology Transactions*, 1996, **39**, 915–921.

13 H. S. Davies, D. Débarre, N. El Amri, C. Verdier, R. P. Richter and L. Bureau, *Physical Review Letters*, 2018, **120**, 198001.

14 S. Leroy, A. Steinberger, C. Cottin-Bizonne, F. Restagno, L. Léger and É. Charlaix, *Physical Review Letters*, 2012, **108**, 264501.

15 Z. Zhang, V. Bertin, M. Arshad, E. Raphael, T. Salez and A. Maali, *Physical Review Letters*, 2020, **124**, 054502.

16 E. Bissett and D. Spence, *Proceedings of the Royal Society of London. A. Mathematical and Physical Sciences*, 1989, **424**, 409–429.

17 Z. Liu, H. Dong, A. Jagota and C.-Y. Hui, *Soft Matter*, 2022.

18 C.-Y. Hui, H. Wu, A. Jagota and C. Khripin, *Tribology Letters*, 2021, **69**, 1–17.

19 H. Wu, N. Moyle, A. Jagota and C.-Y. Hui, *Soft matter*, 2020, **16**, 2760–2773.

20 J. H. Snoeijer, J. Eggers and C. H. Venner, *Physics of Fluids*, 2013, **25**, 101705.

21 M. H. Essink, A. Pandey, S. Karpitschka, C. H. Venner and J. H. Snoeijer, *Journal of Fluid Mechanics*, 2021, **915**, A49.

22 K. Sekimoto and L. Leibler, *Europhysics Letters*, 1993, **23**, 113.

23 J. M. Skotheim and L. Mahadevan, *Physics of Fluids*, 2005, **17**, 092101.

24 T. Salez and L. Mahadevan, *Journal of Fluid Mechanics*, 2015, **779**, 181–196.

25 V. Bertin, Y. Amarouchene, E. Raphael and T. Salez, *Journal of Fluid Mechanics*, 2022, **933**, A23.

26 J. M. Skotheim and L. Mahadevan, *Physical Review Letters*, 2004, **92**, 245509.

27 J. Urzay, S. G. Llewellyn Smith and B. J. Glover, *Physics of Fluids*, 2007, **19**, 103106.

28 B. Saintyves, T. Jules, T. Salez and L. Mahadevan, *Proceedings of the National Academy of Sciences*, 2016, **113**, 5847–5849.

29 B. Saintyves, B. Rallabandi, T. Jules, J. Ault, T. Salez, C. Schönecker, H. A. Stone and L. Mahadevan, *Soft matter*, 2020, **16**, 4000–4007.

30 T. G. J. Chandler and D. Vella, *Proceedings of the Royal Society A*, 2020, **476**, 20200551.

31 A. Kargar-Estahbanati and B. Rallabandi, *Physical Review Fluids*, 2021, **6**, 034003.

32 S. Leroy and E. Charlaix, *Journal of Fluid Mechanics*, 2011, **674**, 389.

33 T. M. Geislinger and T. Franke, *Advances in Colloid and Interface Science*, 2014, **208**, 161–176.

34 Y. Peng, C. M. Serfass, A. Kawazoe, Y. Shao, K. Gutierrez, C. N. Hill, V. J. Santos, Y. Visell and L. C. Hsiao, *Nature Materials*, 2021, **20**, 1707–1711.

35 J. De Vicente, J. Stokes and H. Spikes, *Tribology Letters*, 2005, **20**, 273–286.

36 J. De Vicente, J. Stokes and H. Spikes, *Food Hydrocolloids*, 2006, **20**, 483–491.

37 A. C. Moore and D. L. Burris, *Journal of Biomechanics*, 2014, **47**, 148–153.

38 D. Burris, L. Ramsey, B. Graham, C. Price and A. Moore, *Tribology Letters*, 2019, **67**, 1–10.

39 B. Rallabandi, B. Saintyves, T. Jules, T. Salez, C. Schönecker, L. Mahadevan and H. A. Stone, *Physical Review Fluids*, 2017, **2**, 074102.

40 K. L. Johnson, *Contact Mechanics*, Cambridge University Press, 1987.

41 E. Bissett, *Proceedings of the Royal Society of London. A. Mathematical and Physical Sciences*, 1989, **424**, 393–407.

42 C. M. Bender and S. A. Orszag, *Advanced Mathematical Methods for Scientists and Engineers I: Asymptotic Methods and Perturbation Theory*, Springer Science & Business Media, 1999, vol. 1.